Micro-Doppler Mini-UAV Classification Using Empirical-Mode Decomposition Features

Article *in* IEEE Geoscience and Remote Sensing Letters · January 2018

DOI: 10.1109/LGRS.2017.2781711

Micro-Doppler mini-UAV Classification Using Empirical Mode Decomposition Features

Beom-Seok Oh, Xin Guo, Fangyuan Wan, Kar-Ann Toh, Zhiping Lin*

***Abstract*—In this letter, we propose an empirical mode decomposition (EMD) based method for automatic multi-category mini-UAV classification. The radar echo signal is firstly decomposed into a set of oscillating waveforms by EMD. Then, eight statistical and geometrical features are extracted from the oscillating waveforms to capture the phenomenon of blade flashes. After feature normalization and fusion, a nonlinear support vector machine is trained for target class label prediction. Our empirical results on real measurement of radar signals show encouraging mini-UAV classification accuracy performance.**

***Index Terms*—Micro-Doppler Signature, Empirical Mode Decomposition, Unmanned Aerial Vehicle Classification**

I. Introduction

DURING the past decade, both the technology and the industry of UAV have advanced greatly. The equipment cost has been significantly lowered while the flying performance of UAVs has been largely enhanced. This advancement enables UAV to be deployed in a wide range of applications (e.g., parcel delivery). On the other hand, UAVs may form a threat to security-sensitive areas if they are used for spying, reconnaissance and even for attack. This is particularly true since existing mini-sized UAVs are difficult to detect due to their small size, slow flying speed and low flying altitude. For those security-sensitive areas, an accurate automatic detection and classification of mini-UAVs is of particular interest.

The radar technology is widely adopted in surveillance systems because it has fast remote sensing capabilities regardless of weather. Among the various signal processing techniques for radar signals, the micro-Doppler signature (m-DS) [1] is the most popular choice for mini-UAV classification [2]–[7]. This is because the m-DS extracted from radar echo signals can capture the unique characteristics of micro-motion induced by the mini-UAV propeller/rotor blades [5]–[7]. Table I shows a summary of existing radar m-DS based state-of-the-art mini-UAV classification methods.

In the two most recent works [6], [7], the authors have reported very good classification performances. However, although a pre-trained convolutional deep network model is utilized in [6], collecting a large enough number of labeled data for deep network tuning is costly. The method proposed in [7] is for a binary-category problem only and it is not straightforward to extend to the multi-category problem. Note that classifying a mini-UAV into its type/model is an important task as different mini-UAV may form a different level of threat.

TABLE I
EXISTING WORKS ON RADAR M-DS BASED MINI-UAV CLASSIFICATION

Authors (year)	Main objective (Num. of target class)	Radar m-DS analysis	Classification
Molchanov et al. (2014) [2]	mini-UAV model/type classification (5 & 11)	Spectrogram	NBC[1], linear & nonlinear SVM[2]
Harmanny et al. (2015) [3]	mini-UAV type classification (5)	Spectrogram, Cepstrogram	Maximum a posteriori
Fioranelli et al. (2015) [4]	mini-UAV payloads classification (2)	Spectrogram	NBC, DDA[3]
Torvik et al. (2016) [5]	Quadcopters vs. birds classification (4)	Radar polarimetry	Nearest neighbor classifier
Kim et al. (2017) [6]	Quadcopter vs. hexacopter (2)	Spectrogram + CVD[4]	Convolutional neural network
Ren and Jiang (2017) [7]	mini-UAV vs. birds classification (2)	2-D complex-log-Fourier transform	Subspace reliability analysis
Proposed method	mini-UAV model classification (2 & 11)	EMD	Nonlinear SVM

[1]NBC: naive Bayes classifier, [2]SVM: support vector machine, [3]DDA: diagonal-linear variant of the discriminant analysis, [4]CVD: cadence-velocity diagram.

Table I also shows that the majority of works in the literature is relying on the short-time Fourier transform (STFT) analysis such as spectrogram. We note that many Fourier analysis based prior arts require signals with a longer dwell time to capture the desired spectral information. Moreover, the time-frequency resolution may pose a limitation for the STFT-based techniques. A simple and yet effective resolution to address these limitations is to analyze the m-DS using a non-Fourier time-frequency analysis method. In this work, we propose to deploy the EMD [8] for the m-DS analysis of mini-UAVs.

The core idea of EMD is to treat the signal as fast oscillations superimposed on slow oscillations. Essentially, the EMD decomposes a real-valued univariate signal $\boldsymbol{x} \in \mathbb{R}^d$ into a set of oscillating waves as: $\boldsymbol{x} = \sum_{l=1}^{L} \boldsymbol{m}_l + \boldsymbol{q}_L$, where $\boldsymbol{m}_l \in \mathbb{R}^d$ indicates the l-th intrinsic mode function (IMF) and $\boldsymbol{q}_L \in \mathbb{R}^d$ is a residue [8]. Each of the obtained IMFs is dominated by certain frequency components. Different from the STFT analysis, the frequency band of each IMF is adaptively determined based on the input signal. Another unique characteristic of the EMD is that the signal is decomposed locally. Our idea behind using the EMD for the mini-UAV radar m-DS analysis is to capture the phenomenon of blade flashes locally and adaptively.

The EMD method has been successfully deployed in a wide range of applications such as speech signal processing [9], fault diagnosis [10], electroencephalography analysis [11], m-DS analysis for classification of large aerial targets (e.g., jet-/ propeller-aircraft and helicopter) [12]–[15], and ground moving vehicle [16]. However, none of the existing works is on mini-UAV classification. While some EMD analysis results on mini-UAV echo signals are presented in [17], their

B.-S. Oh, F. Wan and Z. Lin are with School of Electrical and Electronic Engineering, Nanyang Technological University, 50 Nanyang Avenue, 639798 Singapore.

X. Guo is with Temasek Laboratories at Nanyang Technological University (TL@NTU), 50 Nanyang Drive, 637553 Singapore.

K.-A. Toh is with School of Electrical and Electronic Engineering, Yonsei University, 50 Yonsei-ro, Seodaemun-gu, Seoul, 03722, Republic of Korea.

The authors thank the Thales Nederland for providing the CW radar data.

* Corresponding author: ezplin@ntu.edu.sg

analysis is limited to signals measured under indoor condition. Moreover, no further study on EMD (e.g., feature extraction and classification) is reported in [17].

Since the radar echo from mini-UAVs is generally much weaker than that from the large manned aerial vehicles, the existing EMD-based works [12]–[16] cannot be directly applied to the mini-UAV classification problem. In [14] and [16], for example, a few statistical features (e.g., entropy, second order moment etc.) were respectively extracted from the first IMF and the sum of the remaining IMFs for classification of large aerial vehicles and ground moving vehicles. However, as shown in Figs. 1 and 2, the first IMF of mini-UAVs' echo contains almost no target information. Our analysis (see Section II for details) shows that the order of IMF in which the blade flash responses appear varies over mini-UAV types. Moreover, the order of blade flash IMF may vary within a mini-UAV type according to the signal quality.

Motivated by the above observations on the EMD properties and in view of the lack of study in mini-UAV classification, in this letter, we propose an EMD based method for mini-UAV classification. Essentially, a radar echo signal is decomposed into a set of IMFs using EMD. Eight statistical and geometrical features, which are designed for label discrimination, are then respectively extracted from the IMFs. After normalization and fusion, the extracted features are used to train a nonlinear SVM classifier for target class label prediction. The main contributions of this letter can be enumerated as follows:

- Proposal of an effective EMD-based method for mini-UAV classification. Four novel geometrical features are proposed and extracted together with four conventional statistical features from a set of IMFs.
- Provision of an empirical analysis on radar mini-UAV m-DS showing the relationships between the spectrogram and the IMFs in terms of the blade flash phenomenon.
- Extraction of three sets of features from a complex-valued signal using the real-valued EMD, and then fuse them for mini-UAV classification performance enhancement.

II. Micro-Doppler signature analysis using EMD

In this section, the effectiveness of using EMD for radar m-DS analysis is empirically investigated. Particularly, the m-DS induced by the micro-motion of three types of mini-UAVs (e.g., helicopter, fixed-wing and quadcopter) is considered. A physically measured continuous-wave (CW) radar echo (see Section IV-A for the radar setup) is firstly analyzed using the STFT which produces a spectrogram, and the EMD which produces a set of IMFs. Both analysis results are then compared to each other in terms of the blade flash phenomenon [1]. The STFT is computed using a sliding Hamming window of length 2^8 with 90% overlapping.

A. Helicopter type mini-UAV

Fig. 1 shows two sets of a spectrogram and the first four IMFs, obtained by analyzing the radar signals (of 50ms long) of a helicopter mini-UAV. In Fig. 1 (a), the spectrogram obtained using the radar echo of a helicopter mini-UAV with strong m-DS is shown. In the subplot, the micro-Doppler spectrum width and blade flashes are clearly visible [1]. Via

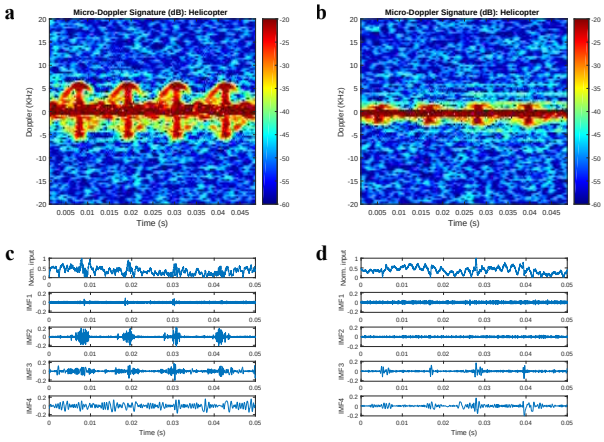

Fig. 1. Two sets of a spectrogram and the first four IMFs obtained using a measurement radar signal ((a) and (c)) with strong m-DS and ((b) and (d)) with weak m-DS (due to different angle of viewing) of a helicopter mini-UAV.

a simple analysis on the blade flashes [18], several physical mini-UAV parameters namely, the number of blades and its length, blade tip velocity, rotation rate and blade symmetry, can be retrieved from the subplot. It should be noted here that, however, such information can be retrieved with a certain accuracy only when the m-DS is strong enough. For example, the spectrogram shown in Fig. 1 (b) is computed using a radar signal of the same mini-UAV model, but with weak m-DS due to different angle of viewing the mini-UAV (e.g., the rotor mast of the helicopter mini-UAV was nearly parallel to the radar line of sight). The mini-UAV parameters retrieved in Fig. 1 (b) might be totally different from those in Fig. 1 (a).

Different from the spectrogram, the IMFs do not possess physical-parameter-specific information. The EMD instead captures existence of blade flashes with time information. Fig. 1 (c) and (d) respectively show the first four IMFs obtained from the two radar signals used to compute the spectrograms shown in Fig. 1 (a) and (b). As shown in Fig. 1 (c), the first IMF (IMF1) oscillates with an almost constant variance over time. On the other hand, the local amplitude of IMF2 changes significantly at certain time points. By synchronizing such amplitude patterns with the spectrogram shown in Fig. 1 (a), it is observed that those blade flashes captured by EMD appear as high amplitude with a small number of zero-crossings within a certain IMF (e.g., IMF2 of Fig. 1 (c)). Even for the weak m-DS as shown in Fig. 1 (d), the IMF3 still contains such blade flash patterns which are useful for classification.

B. Fixed-wing type and Quadcopter type mini-UAVs

We now consider two different types of mini-UAV, namely a fixed-wing type (see Fig. 2 (a) and (c)) and a quadcopter type (Fig. 2 (b) and (d)). Due to space constraint, only radar signals with strong m-DS are shown here. Similar to those IMFs shown in Fig. 1 (c), the blade flashes induced by these two mini-UAV types appear at IMF4 (see Fig. 2 (c)) and at IMF3 (see Fig. 2 (d)), respectively. The main reason for observing such responses from different orders of IMF is due to different characteristics of rotor blades. For example, in general, the main rotor blades of a helicopter mini-UAV are much longer and wider than that of a fixed-wing and a quadcopter mini-UAV. Such physical differences in blades

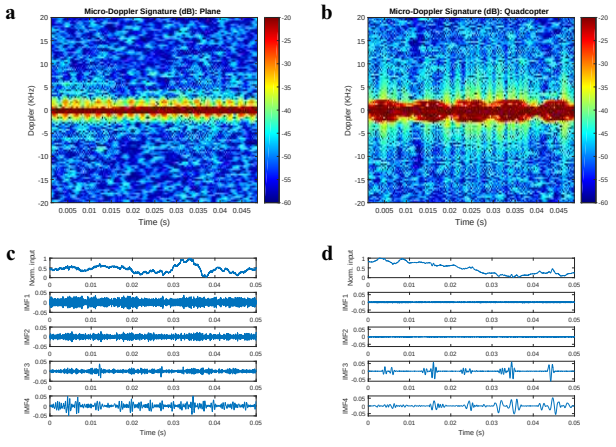

Fig. 2. Two sets of a spectrogram and the first four IMFs obtained using a measurement radar signal of ((a) and (c)) a fixed-wing mini-UAV and ((b) and (d)) a quadcopter mini-UAV.

affect the return signals, and thus micro-Doppler frequency. This is an important property for mini-UAV classification.

III. Proposed Method for Mini-UAV Classification

We have empirically shown in Section II that the EMD can effectively capture the unique patterns of m-DS induced by the micro-motion of mini-UAV blades. To extract and utilize such unique information for mini-UAV classification, in this section, we propose to extract eight statistical and geometrical features from the obtained IMFs. After normalization and fusion, the obtained features are used to train a nonlinear SVM classifier.

A. Features extraction from IMFs and Normalization

Let $\boldsymbol{s}_i \in \mathbb{C}^d$, $i = 1, \cdots, m$, denotes the i-th univariate radar signal, where m indicates the total number of training samples. Since $\boldsymbol{s}_i$ is complex-valued, it is firstly converted to a real-valued signal $\boldsymbol{x}_i = |\boldsymbol{s}_i| \in \mathbb{R}^d$, where $|\cdot|$ indicates the magnitude function. The EMD decomposes $\boldsymbol{x}_i$ into L number of IMFs $\boldsymbol{m}_l^i$ and a residue $\boldsymbol{q}_L^i$. For simplicity, $\boldsymbol{m}_l^i$ will be denoted as $\boldsymbol{m}_l$ hereafter unless otherwise specified. The number of resulted IMFs, L, varies according to the frequency contents contained in the signal $\boldsymbol{x}_i$. In this work, only the first $K < L$ IMFs are used for extraction of the eight features listed in Table II.

Features 1 to *4* are the conventional statistical features adopted from the literature while *Features 5* to *8* are geometrical features newly proposed in this work. *Features 6* and *7* are designed to geometrically capture the blade flash responses (see Fig. 1 (c) and (d)) within the IMFs while *Features 5* and *8* are for capturing geometrical relationships between two consecutive IMFs. These new features are chosen because the blade flash response and its geometrical relationship information cannot be found in the literature.

The extracted eight feature vectors are subsequently concatenated: $\boldsymbol{f}_i = \left[\boldsymbol{f}_{i,1}^T, \boldsymbol{f}_{i,2}^T, \cdots, \boldsymbol{f}_{i,8}^T\right]^T \in \mathbb{R}^{8K-2}$, and then stacked into a matrix form: $\boldsymbol{F}^{Mag} = [\boldsymbol{f}_1, \boldsymbol{f}_2, \cdots, \boldsymbol{f}_m] \in \mathbb{R}^{(8K-2)\times m}$. For the subsequent classification process, each row vector of $\boldsymbol{F}^{Mag}$ is normalized to within the range of $[0,1]$ using the min-max normalization technique. Since the test data is not available beforehand, its features can only be normalized with respect to the min and max values of the training features.

B. Feature level fusion of the EMD features

It is observed from our preliminary results that the information contained in the eight features may not be enough to produce a good accuracy performance. Particularly, feature vector $\boldsymbol{f}_i \in \mathbb{R}^{8K-2}$ extracted at $K = 6$ and from a 50ms signal $\boldsymbol{x}_i \in \mathbb{R}^{4,800}$, is just of 46 dimension. To enhance the classification accuracy performance, we propose to extract two more sets of the eight features namely, $\boldsymbol{F}^{Real}$ from $Real(\boldsymbol{s}_i)$ and $\boldsymbol{F}^{Imag}$ from $Imaginary(\boldsymbol{s}_i)$, together with $\boldsymbol{F}^{Mag}$ extracted from $|\boldsymbol{s}_i|$. The fused feature is defined as follows: $\boldsymbol{F}^{Fusion} = [(\boldsymbol{F}^{Mag})^T, (\boldsymbol{F}^{Real})^T, (\boldsymbol{F}^{Imag})^T]^T \in \mathbb{R}^{3(8K-2)\times m}$.

C. Mini-UAV classification using the RBF-SVM classifier

The extracted feature matrix, $\boldsymbol{F}^{Mag}$ or $\boldsymbol{F}^{Fusion}$, is then used to train the SVM with a nonlinear radial basis function (RBF) kernel. To handle the multi-categories, the SVM is trained with the one-vs-all learning scheme. This nonlinear SVM classifier is adopted due to its strong theoretical foundations with guaranteed reliable classification performance. Due to space constraint, we refer to [20] for more details on the SVM.

IV. Experiments

The main goal of this study is to empirically verify the effectiveness of the proposed method for mini-UAV classification. To achieve this goal, a set of real radar signals returned from 11 objects, is utilized in this experimental study. The resulted accuracy performance is then compared with that of competing state-of-the-arts. The following subsections provide the details of our dataset, experimental setup and results.

A. Dataset and Preprocessing

As shown in Table III, the dataset consists of eleven object models including six commercial mini-UAVs. This dataset, provided by Thales Nederland, was collected at outdoors using an X-band CW radar (9.7GHz radio frequency, 192KHz sampling rate). A horn antenna was manually adjusted towards the nearby target object (see the fourth column of Table III for the distance range between the radar and target object). The radar signal is decimated by a factor of two to reduce the sampling rate to 96KHz. The identified valid signals are then divided into non-overlapping segments of $\{20, 30, \cdots, 100\}$ms long (a.k.a. dwell time) similar to that in [2]. This is to observe the relationship among the dwell time, the accuracy performance and the number of IMFs, K. In [2], Molchanov et al.'s method, which was STFT-based, worked well only for segments with longer dwell time (>100ms). Since our proposed method is non-Fourier based, we are particularly interested in investigating the shortest possible working range for the dwell time. Through this range study, the relationship between the minimum number of IMFs K and the dwell time can be explored. In field application, a proper value for the dwell time can be found based on a cross-validation test using the accumulated training data.

B. Evaluation of the proposed method (11-category problem)

1) Experimental setup: The main objective here is to classify an unseen test sample into one of the eleven categories shown in Table III. The proposed method has two adjustable

TABLE II
THE EIGHT STATISTICAL (FEATURES 1 TO 4) AND GEOMETRICAL (FEATURES 5 TO 8) FEATURES TO BE EXTRACTED FROM IMFS, $\boldsymbol{m}_l$ WHERE $l = 1,\cdots,K$

No.	Brief description	Feature	Details / Note
1	Number of zero crossing [19]	$\boldsymbol{f}_{i,1} = [Z_1,\cdots,Z_K]^T \in \mathbb{R}^K$	$Z_l = \sum_{n=2}^{d} \lvert sign[m_l(n)] - sign[m_l(n-1)]\rvert$, $sign[m_l(n)] = 1$ if $m_l(n) \geq 0$, otherwise 1. $\boldsymbol{m}_l = [m_l(1),\cdots,m_l(d)]^T$
2	Normalized signal energy [10], [16]	$\boldsymbol{f}_{i,2} = [E_1/E,\cdots,E_K/E]^T \in \mathbb{R}^K$	$E_l = \sum_{n=1}^{d} \lvert m_l(n)\rvert^2$ is the signal energy of $\boldsymbol{m}_l$, $E = \sum_{l=1}^{K} E_l$
3	Standard deviation [20]	$\boldsymbol{f}_{i,3} = [std(\boldsymbol{m}_1),\cdots,std(\boldsymbol{m}_K)]^T \in \mathbb{R}^K$	$std(\boldsymbol{m})$ returns the standard deviation of $\boldsymbol{m}$
4	Entropy (see chapter 11 of [21])	$\boldsymbol{f}_{i,4} = [En(\boldsymbol{m}_1),\cdots,En(\boldsymbol{m}_K)]^T \in \mathbb{R}^K$	$En(\boldsymbol{m}_l) = -\sum P(\boldsymbol{m}_l)\log_2 P(\boldsymbol{m}_l)$ and $P(\cdot)$ returns the histogram counts of $\boldsymbol{m}_l$ with 256 bins
5	Entropy of two concatenated IMFs	$\boldsymbol{f}_{i,5} = [En(\boldsymbol{m}'_1),\cdots,En(\boldsymbol{m}'_{K-1})]^T \in \mathbb{R}^{K-1}$	$\boldsymbol{m}'_l = [\boldsymbol{m}_l^T, \boldsymbol{m}_{l+1}^T]^T$: a concatenation of two consecutive IMFs
6	Normalized max-mean difference	$\boldsymbol{f}_{i,6} = [D_1,\cdots,D_K]^T \in \mathbb{R}^K$	$D_l = \frac{\max_\gamma(\boldsymbol{m}_l) - mean(\boldsymbol{m}_l > 0)}{\max_\gamma(\boldsymbol{m}_l)}$, $\max_\gamma(\boldsymbol{m}_l)$ returns the γ-th maximum value of $\boldsymbol{m}_l$, and $mean(\cdot)$ denotes the mean function. The γ is used to remove exceptional outliers
7	Distance between two frequency peaks	$\boldsymbol{f}_{i,7} = [P_1,\cdots,P_K]^T \in \mathbb{R}^K$	$P_l = \frac{\lvert \arg\max(F_l) - d/2\rvert \times 2}{d}$, $F_l = \sum_{f=-\infty}^{\infty} \lvert M_l(f)\rvert^2$, and $M_l(f)$ indicates the Fourier transform of $m_l(n)$
8	Ratio of zero-crossing number Z_l	$\boldsymbol{f}_{i,8} = [Z_2/Z_1,\cdots,Z_K/Z_{K-1}]^T \in \mathbb{R}^{K-1}$	Refer to *Feature 1* for details of Z_l

TABLE III
SPECIFICATIONS OF THE REAL MEASUREMENT DATASET

No.	Target object name	Target object type	Distance range to the target†	Num. segments (50ms long)
1	Birds	non-UAV	5m–50m	1,129
2	Yak54	Fixed-wing	20m–150m	1,480
3	EasyStar			780
4	T-REX450	Helicopter	20m–70m	1,759
5	Logo 400			1,141
6	Logo 600			717
7	Parrot 2.0	Quadcopter	3m–20m	3,534
8 / 9	1 / 2 rotors	Stationary rotor	5m, 10m, 15m, 20m for each	298 / 336
10/11	3 / 4 rotors			240 / 600

†Since the CW radar cannot measure the target distance range, the distance range was estimated based on the land size of the mini-UAV trial field, and based on those video recordings which were acquired together with the radar data.

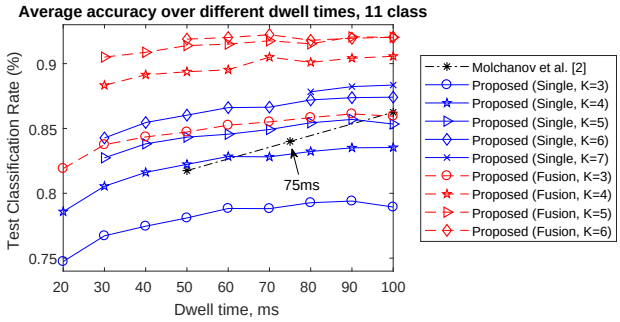

Fig. 3. Performances of the proposed method at $K \in \{3,\cdots,7\}$ and at $\sigma = 7$. The extractable K varies according to the frequency contents contained in the signal (e.g., 7 IMFs can be extracted only when the dwell time $\geq$ 80ms).

parameters namely, the number of IMFs K used for feature extraction, and the RBF kernel width σ for the adopted nonlinear SVM classifier. Since the K is closely related to the dimension of the extracted features, the proposed method shall be evaluated over various $K \in \{3,\cdots,7\}$ settings. Different from the K, an optimal value for $\sigma = 7$ is chosen among $\{0.1, 1, 5 : 2 : 19, 50, 100\}$ in terms of random 10 runs of 2 folds cross-validation tests using only the training set. The stopping criterion for computing each IMF is fixed at 10 iterations [22].

The test classification accuracy performance is computed as $\frac{\text{The number of correctly matched test samples}}{\text{Total number of test samples}}$. For statistical evidence, a test based on random 20 runs of 10 fold cross-validation is performed, where the average is recorded. All experiments were performed on a PC (3.2GHz, 8G RAM) under the Matlab platform. The Matlab code for EMD is obtained from [22].

2) Results and discussions: Fig. 3 shows the test average accuracy values of the proposed method obtained at $K \in \{3,\cdots,7\}$, which are plotted over different dwell times. To position the proposed method among those competing mini-UAV classification methods, its test accuracy is compared with that of Molchanov et al.'s work [2]. Since the classification results reported in [2] were obtained using the same dataset except for certain protocol details (e.g., sampling rate, signal normalization and cropping), the directly taken accuracy values at $\{50\text{ms}, 75\text{ms}, 100\text{ms}\}$ from [2] are shown in the plot.

Fig. 3 shows that the proposed method before fusion (denoted as 'Proposed (Single)') outperforms the compared Molchanov et al.'s method when $K \in \{6,7\}$ IMFs are utilized for feature extraction. Interestingly, the performance gap is observed to be larger when the dwell time is shorter (e.g., 50ms). After the feature level fusion ('Proposed (Fusion)'), the proposed method for $K > 3$ produces higher accuracies than those of Molchanov et al.'s method. From the confusion matrix of the 'Proposed (Fusion, $K = 6$ at 70ms)' as shown in Table IV, it is observed that most of the errors occur from categories 3 and 10. About 7–8.5% of the fixed-wing echos (categories 2 and 3) are also wrongly classified as a quadcopter (category 7). Particularly, when the radar echo signals contain weak blade flashs and/or similar blade flash patterns over categories (e.g., 2 and 3), our method produces incorrect classification since the eight features are only sensitive to the blade flash patterns from the IMFs.

TABLE IV
CONFUSION MATRIX (%) OF THE 'PROPOSED (FUSION, K=6 AT 70MS)'

		Estimated class label										
		1	2	3	4	5	6	7	8	9	10	11
True	1	**99**	0.4	0	0	0	0	0.6	0	0	0	0
	2	1.1	**86.3**	5.5	0.1	0.1	0	6.9	0	0	0	0
	3	1.9	31.4	**58.1**	0	0.1	0	8.5	0	0	0	0
	4	0.1	1.9	0.1	**96.1**	1.2	0.1	0.5	0	0	0	0
	5	0.1	0.4	0.2	1.4	**97.9**	0	0	0	0	0	0
	6	0.6	0	0	0.2	0.1	**99.1**	0	0	0	0	0
	7	0.7	0.1	0.3	0	0	0	**98.9**	0	0	0	0
	8	1.4	0	0	0	0	0	0	**95.6**	3.0	0	0
	9	0.9	0	0	0	0	0	1	3.3	**94.6**	0	0.2
	10	1.8	0	0	0	0	0	2.5	0.9	6.7	**66.2**	21.9
	11	0.7	0	0	0.4	0	0	0	0	1.3	4.4	**93.2**

Fig. 4 shows the average test classification accuracies

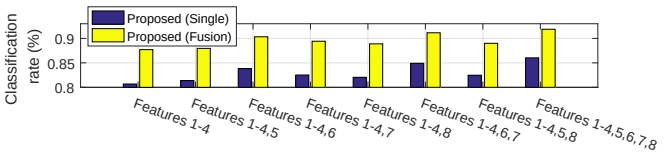

Fig. 4. The impact of the proposed features on the classification accuracy performance (%) at a dwell time of 50ms and $K = 6$. For example, the '*Features 1–4,6*' means five features (*Features 1, 2, 3, 4* and *6*) are utilized

TABLE V
COMPARISON BETWEEN THE PROPOSED METHOD AND COMPETING STATE-OF-THE-ARTS. AVERAGE TEST RESULTS TAKEN OVER RANDOM 20 RUNS OF 2 FOLD CROSS-VALIDATION TESTS USING 50MS SIGNAL

Method	EER	$\text{FAR}_{FRR=1\%}$
Spectrogram+PCA†	7.75	27.00
CVD+PCA†	6.68	28.41
Cepstrogram+PCA†	10.17	48.07
2D complex-log-Fourier transform+PCA† [7]	3.98	4.50
2D complex-log-Fourier transform+SRA† [7]	3.27	3.89
Proposed (Single, $K = 4$)	3.54	4.78
Proposed (Fusion, $K = 4$)	3.43	4.67

†The error rates are directly taken from [7]. Note that all the error rates listed in this table were obtained using the identical data and protocols.

obtained over different combinations of the features. It is observed from Fig. 4 that each of the proposed features contains uncorrelated and discriminative information. Due to the inclusion of more blade-flash-related information from *Features 5–8*, our method achieves the best accuracy performance, which is about 4–5% higher than that of using only the four statistical features ('*Features 1–4*').

C. Comparison with state-of-the-arts (2-category problem)

As shown in Table V, the proposed method is now compared with competing state-of-the-arts (e.g., the 2D complex-log-Fourier transform [7] and the subspace reliability analysis (SRA) [7]) under a binary classification problem. Note that the dataset utilized in [7] is exactly the same with that of ours. Following the experimental protocols reported in [7], the equal error rate (EER) and the false acceptance rate when the false rejection rate equals to 1% ($\text{FAR}_{FRR=1\%}$) of the proposed method are obtained (see Table V). These error rates are then compared with those taken directly from [7]. Different from the results shown in Fig. 3, the proposed method achieves the best error rates at $K = 4$, which appear to be similar to (or slightly worse than) those of the 2D complex-log-Fourier based methods [7]. However, as aforementioned, the methods proposed in [7] were for a binary-category problem only and it is not clear how to extend to the multi-category problem. The table also shows that our method significantly outperforms the spectrogram, CVD and cepstrogram based methods.

V. CONCLUSION

In this letter, an EMD based method was proposed for mini-UAV classification. The radar echo signal was decomposed into a set of IMFs for m-DS estimation. From our empirical analysis, it was observed that blade flashes appeared as sharp changes towards high magnitudes with fewer number of zero-crossings than those time segments without such blade flashes. Moreover, the order of IMF's, in which such responses appear, was observed to be different across mini-UAV types. To extract such information, eight statistical and geometrical features were extracted from the first few IMFs. After normalization and fusion, the extracted features were classified using the SVM classifier. Our empirical results on physical radar signals showed comparable or better accuracy performance than competing state-of-the-arts for mini-UAV classification.

REFERENCES

[1] V. C. Chen, *The micro-Doppler Effect in radar*. Artech House, 2011.
[2] P. Molchanov, R. I. A. Harmanny, J. J. M. de Wit, K. Egiazarian, and J. Astola, "Classification of small UAVs and birds by micro-Doppler signatures," *Int. J. Microw. Wirel. T.*, vol. 6, no. 3-4, pp. 435–444, 2014.
[3] R. I. A. Harmanny, J. J. M. de Wit, and G. Premel-Cabic, "Radar micro-Doppler mini-UAV classification using spectrograms and cepstrograms," *Int. J. Microw. Wirel. T.*, vol. 7, no. 3-4, pp. 469–477, 2015.
[4] F. Fioranelli, M. Ritchie, H. Griffiths, and H. Borrion, "Classification of loaded/unloaded micro-drones using multistatic radar," *Electron. Lett.*, vol. 51, no. 22, pp. 1813–1815, 2015.
[5] B. Torvik, K. E. Olsen, and H. Griffiths, "Classification of Birds and UAVs Based on Radar Polarimetry," *IEEE Geosci. Remote Sens. Lett.*, vol. 13, no. 9, pp. 1305–1309, 2016.
[6] B. K. Kim, H.-S. Kang, and S.-O. Park, "Drone classification using convolutional neural networks with merged doppler images," *IEEE Geosci. Remote Sens. Lett.*, vol. 14, no. 1, pp. 38–42, 2017.
[7] J. Ren and X. Jiang, "Regularized 2-d complex-log spectral analysis and subspace reliability analysis of micro-doppler signature for uav detection," *Pattern Recogn.*, vol. 69, pp. 225–237, 2017.
[8] N. E. Huang, Z. Shen, S. R. Long, M. C. Wu, H. H. Shih, Q. Zheng, N.-C. Yen, C. C. Tung, and H. H. Liu, "The empirical mode decomposition and the Hilbert spectrum for nonlinear and non-stationary time series analysis," in *Proc. Roy. Soc. London Ser. A*, vol. 454, no. 1971, 1998, pp. 903–995.
[9] A. Bouzid and N. Ellouze, "Empirical Mode Decomposition of Voiced Speech Signal," in *Proc. Int. Symp. Control, Commun. Sig. Proc.* IEEE, 2004, pp. 603–606.
[10] Y. Yu, Y. Dejie, and C. Junsheng, "A roller bearing fault diagnosis method based on EMD energy entropy and ANN," *J. sound vib.*, vol. 294, no. 1, pp. 269–277, 2006.
[11] F. Riaz, A. Hassan, S. Rehman, I. K. Niazi, and K. Dremstrup, "EMD-Based Temporal and Spectral Features for the Classification of EEG Signals Using Supervised Learning," *IEEE Trans. Neural Syst. Rehabil. Eng.*, vol. 24, no. 1, pp. 28–35, 2016.
[12] X. Bai, M. Xing, F. Zhou, G. Lu, and Z. Bao, "Imaging of Micromotion Targets With Rotating Parts Based on Empirical-Mode Decomposition," *IEEE Trans. Geosci. Remote Sens.*, vol. 46, no. 11, pp. 3514–3523, 2008.
[13] C. Cai, W. Liu, J. S. Fu, and Y. Lu, "Radar Micro-Doppler Signature Analysis with HHT," *IEEE Trans. Aerosp. Electron. Syst.*, vol. 2, no. 46, pp. 929–938, 2010.
[14] L. Du, B. Wang, Y. Li, and Hongwei, "Robust Classification Scheme for Airplane Targets With Low Resolution Radar Based on EMD-CLEAN Feature Extraction Method," *IEEE Sensors J.*, vol. 13, no. 12, pp. 4648–4662, 2013.
[15] Y. Wang, X. Wu, W. Li, Z. Li, Y. Zhang, and J. Zhou, "Analysis of micro-Doppler signatures of vibration targets using EMD and SPWVD," *Neurocomputing*, vol. 171, pp. 48–56, 2016.
[16] Y. Li, L. Du, and H. Liu, "Hierarchical Classification of Moving Vehicles Based on Empirical Mode Decomposition of Micro-Doppler Signatures," *IEEE Trans. Geosci. Remote Sens.*, vol. 51, no. 5, pp. 3001–3013, 2013.
[17] A. Brewster and A. Balleri, "Extraction and analysis of micro-Doppler signatures by the Empirical Mode Decomposition," in *Proc. IEEE Radar Conf.*, 2015, pp. 0947–0951.
[18] D. Tahmoush, "Detection of small UAV helicopters using micro-Doppler," in *Proc. SPIE Defen. Secur.* International Society for Optics and Photonics, 2014, pp. 907 717–907 717.
[19] S. Baykut and T. Akgül, "Multiscale zero-crossing statistics of intrinsic mode functions for white Gaussian noise," in *Proc. European Sig. Proc. Conf.*, 2010, pp. 135–138.
[20] R. O. Duda, P. E. Hart, and D. G. Stork, *Pattern classification.* John Wiley & Sons, 2012.
[21] R. C. Gonzalez, R. E. Woods, and S. L. Eddins, *Digital Image Processing Using MATLAB.* Third New Jersey: Prentice Hall, 2003.
[22] P. Flandrin, "Empirical Mode Decomposition," http://perso.ens-lyon.fr/patrick.flandrin/emd.html, [Online; accessed 2-October-2016].